Journal of Ceramic Processing Research. Vol. 25, No. 4, pp. 617~623 (2024)
(Received 29 March 2024, Received in revised form 13 July 2024, Accepted 31 July 2024)
https://doi.org/10.36410/jcpr.2024.25.4.617

J O U R N A L O F
Ceramic Processing Research

Color-tunable nanopigments of ZnS_xSe_{1-x}: Preparation, optical properties, and first-principles evaluation

Ti Zhang[b,c], Yanmin Wang[a,*], Shanjun Ke[b,c,*] and Zhidong Pan[a]
[a]*South China University of Technology, Guangzhou 510640, China*
[b]*Foshan Oceano Ceramics Co. Ltd., Foshan 528138, China*
[c]*Guangxi Oceano Ceramics Co. Ltd., Wuzhou 543300, China*

In this work, the effects of the crystalline structure and charge state distribution on the bandgap, dominant wavelength, and optical properties of ZnS_xSe_{1-x} color-tunable nanopigments were investigated for the first time. The first-principles calculation results of ZnS_xSe_{1-x} pigment based on density functional theory demonstrate that ZnS_xSe_{1-x} becomes a material with an adjustable optical bandgap due to the similarity of S and Se. Furthermore, the ZnS_xSe_{1-x} pigment color gradually changed from ivory white to bright yellow with increasing anion composition of x = [S]/([S] + [Se]), thereby obtaining tunable colors and optical properties to meet visual and aesthetic requirements.

Keywords: ZnS_xSe_{1-x}, Optical properties, Kubelka-Munk theory, First-principles evaluation.

Introduction

Recently, inorganic nanopigments [1-5] with tunable colors [6, 7], aesthetic features [8], and nontoxic elements [9, 10] have become important candidates for thermal reflection cold materials in reducing the energy consumption of buildings [11-13]. Inorganic pigments can obtain different colors through selective absorption and reflection in the visible light region [14, 15]. The rational design of pigment compositions produces diversified colors to develop tunable colorful pigments [16].

With high solar/near-infrared (NIR) reflectance, low cost and color-turntable properties, ZnS_xSe_{1-x} has been paid much attention as a novel cool pigments. It can be applied to the complex inorganic color pigments (CICP), ceramic tiles, cool coatings and many others fields. The optical properties of ZnS/ZnSe systems are closely related with their band structure [17-20]. The bandgap of ZnS_xSe_{1-x} is affected by phase structure and the component ratios (x). The bandgap width and the energy levels between the conduction band and the valence band will have an affect on the color-turntable properties of the ZnS_xSe_{1-x} systems.

In this paper, we have aimed at exploring the Kubelka–Munk optical properties and band structure of ZnS_xSe_{1-x} pigments with a controllable crystalline structure and optical properties. The effects of the crystalline structure and charge state distribution on the bandgap, dominant wavelength, and optical properties of ZnS_xSe_{1-x} pigments were initially explored.

*Corresponding author:
Tel : +86 20 87114883
Fax: +86 20 87110273
E-mail: wangym@scut.edu.cn (Y. Wang),
sjkescut@163.com (S. Ke)

Experimental

Synthesis

ZnS_xSe_{1-x} pigments (x = 1, 0.75, 0.55, and 0.35) were synthesized by a coprecipitation reaction and subsequent calcination (Fig. A1) using $ZnSO_4{\cdot}7H_2O$ (99.5%), $Na_2S{\cdot}9H_2O$ (98%), and Se (99%), NaOH (97%) as starting materials supplied by Sinopharm Group Co. Ltd., China. The value of x changes for compositions of ZnS_xSe_{1-x} precursors (see Table A1).

Theoretical method

The CASTEP package was employed to calculate the band structure of ZnS_xSe_{1-x} using first-principle calculations based on density functional theory (DFT). The geometric structure optimization of $ZnS_{0.35}Se_{0.65}$ was first performed by Perdew–Burke–Eruzerh (PBE) in the generalized gradient approximation (GGA) scheme to exchange–correlation effects, and ultrasoft pseudopotentials were used for electron interactions. In addition, the calculation functional used is PBE. A plane-wave cutoff energy of 460 eV was employed in the calculations, which assured a total energy convergence of 2.0×10^{-6} eV/atom. In order to build $ZnS_{0.35}Se_{0.65}$ crystals, the ZnS crystal was initially built as a basic model [21]. $ZnS_{0.35}Se_{0.65}$ was set up using GGA by changing the composition of S atoms by substituting 65% virtual Se atoms. The Brillouin zone (BZ) was set with the 6 × 6 × 6 Monkhorst–Pack k–point meshes (Fig. A2). Zn $3d^{10}4s^2$,

S $3s^2 3p^4$, and Se $4s^2 4p^4$ were considered the valence states, respectively, and the electrons of the remaining orbitals are described by frozen-core approximation.

Characterizations

The crystalline phases of samples were examined on an X-ray diffractometer (PW-1710, Netherlands). The Fourier transform infrared spectra of samples were recorded on a Fourier infrared spectrometer (VERTEX 33, USA) in a frequency range of 400–4000 cm^{-1}. Moreover, X-ray photoelectron spectroscopy (ESCALAB 250Xi, USA) and ultraviolet–visible–near-infrared (UV–vis–NIR) spectrophotometer (LAMBDA 950, USA) were used to determine the element valence state and diffuse reflectance of samples, respectively, using $BaSO_4$ as a reference.

Results and Discussion

Crystalline structure analysis

Fig. 1 presents the Fourier-transform infrared (FTIR) spectra of ZnS_xSe_{1-x} pigments after annealing at 600°C. The FTIR spectra have sharp peaks at 1110 and 672 cm^{-1}, assigned to the vibration of Zn–S and Zn–Se bonds (see Table 1), respectively. It was confirmed that a ZnS_xSe_{1-x} solid solution was formed in the samples.

Fig. A2 shows the X-ray diffraction patterns of ZnS_xSe_{1-x} (x = 1, 0.75, 0.55, and 0.35) pigments after annealing at 600°C. The possible reaction equation is as follows:

$$3Se + 6NaOH \xrightarrow{\Delta} 2Na_2Se + Na_2SeO_3 + 3H_2O \quad (1)$$

$$2ZnSO_4 + Na_2S + Na_2Se \xrightarrow{\Delta} ZnS\downarrow + ZnSe\downarrow + 2Na_2SO_4 \quad (2)$$

$$ZnS + ZnSe \xrightarrow{600℃} Zn(S_xSe_{1-x}) \quad (3)$$

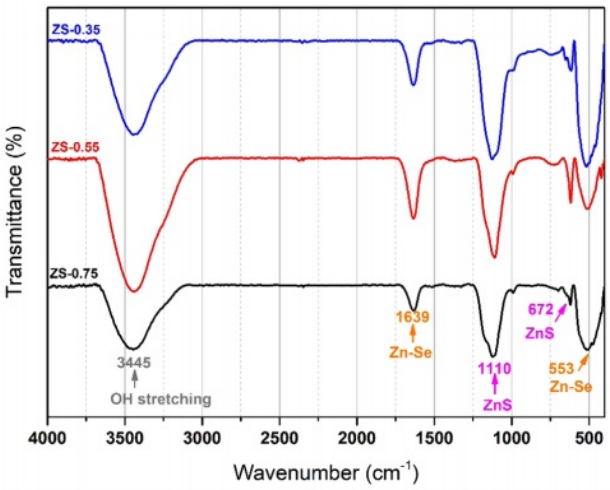

Fig. 1. Fourier-transform infrared spectra of ZnSxSe1−x pigments.

With an increase in Se content in ZnS_xSe_{1-x}, the (111) and (220) crystal planes of ZnS_xSe_{1-x} move in the direction of lower 2θ values, and the lattice parameters also increase (see Table 2).

First-principles study

The ideal zinc blende structure of ZnS and ZnSe belong to the cubic crystal system, F-43 m (no. 216) lattice group. The unit cell structure model following first-principles calculations is shown in Fig. 2, where the composition of S atoms in ZnS varies by substituting 65% virtual Se atoms. Furthermore, the unit cell parameter a of $ZnS_{0.35}Se_{0.65}$ is 5.497 Å, and the unit cell volume is 166.10 Å. The error between the unit cell parameter a and experimental test value (ZS-0.35, a = 5.6672 Å, Table 1) is 3.0%, which is within the allowable error range (±5%).

The calculated band structure of $ZnS_{0.35}Se_{0.65}$ based on the first principles is shown in Fig. 3. The bottom and

Table 1. Fourier-transform infrared peak assignments of ZnS_xSe_{1-x} pigments.

No.	Peak assignment	Wavenumber (cm^{-1})	Wavenumber range (cm^{-1})
1	Stretching vibration of O–H	3445	3440-3450 [22]
2	Zn–Se vibration	1639	1639 [23]
3	Zn–S vibration	1110	1110, 1113 [24]
4	Zn–S vibration	672	672 [24]
5	Stretching vibration of Zn–Se	553	537-553 [23]

Table 2. Variation in lattice parameters and average crystallite size with Se concentrations.

Samples	2θ	Lattice parameter (a = b = c) (Å)	Lattice volume ($Å^3$)	Average crystallite size (D_{111}) (nm)
ZnS	28.358	5.4092	158.27	10.5
ZS-0.75	28.149	5.4901	165.48	27.5
ZS-0.55	27.783	5.5465	170.63	12.7
ZS-0.35	27.224	5.6672	182.01	46.8

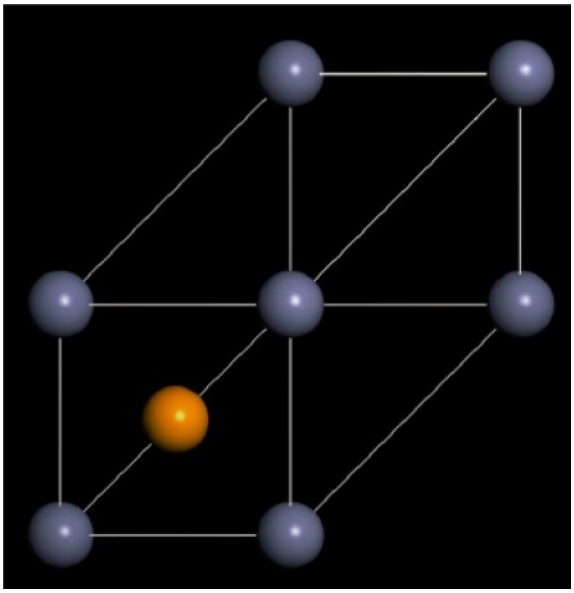

Fig. 2. Cell structure of $ZnS_{0.35}Se_{0.65}$ calculated on the basis of first principles.

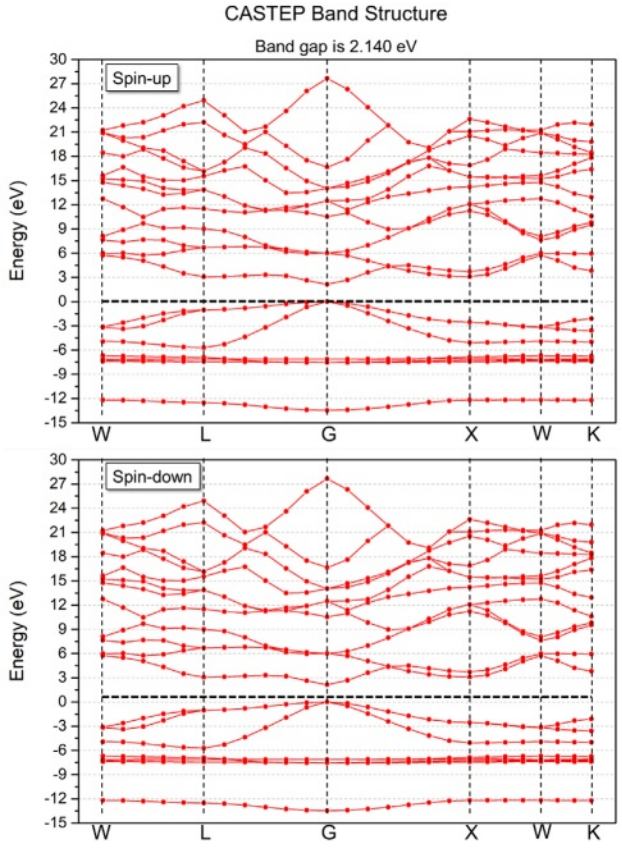

Fig. 3. Band structure of $ZnS_{0.35}Se_{0.65}$ based on first principles (Fermi-level E_F is set to zero energy, which is represented by the horizontal black dashed lines).

top of the conduction and valence bands of $ZnS_{0.35}Se_{0.65}$, respectively, are located at point G in the BZ after setting the Fermi level E_F = 0 eV. Moreover, $ZnS_{0.35}Se_{0.65}$ has

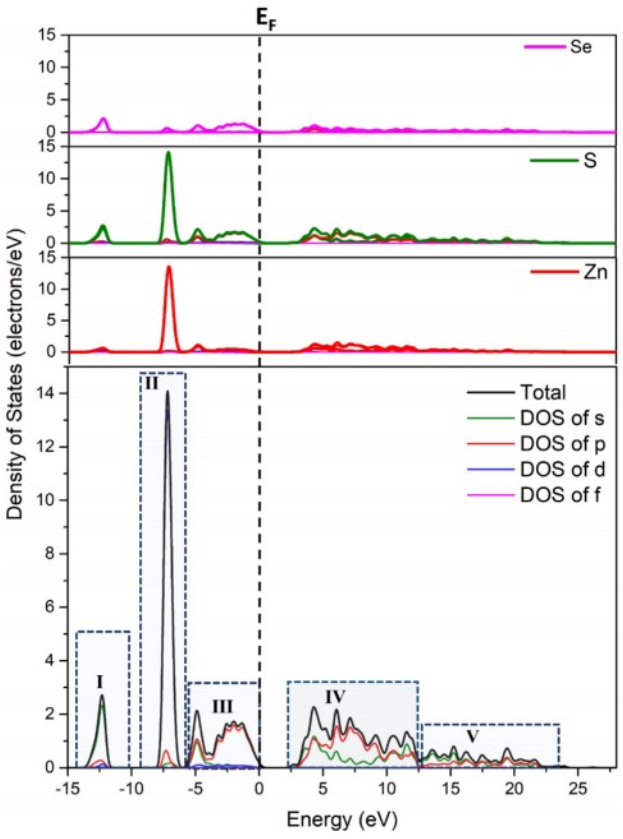

Fig. 4. Total state density and partial state density of $ZnS_{0.35}Se_{0.65}$ single cell (Fermi level E_F is set to zero energy which is denoted by black vertical dashed lines).

an indirect electronic transition type, signifying that ZnS_xSe_{1-x} is a direct bandgap semiconductor material with a tunable optical bandgap [25]. The calculated bandgap value of $ZnS_{0.35}Se_{0.65}$ is 2.140 eV, which is lower [26] than the experimental test value (ZS-0.35, E_g = 2.68 eV, Table 3). The total state density distribution of $ZnS_{0.35}Se_{0.65}$ and partial state density distribution of Zn, S, and Se were calculated to determine the electronic contribution near the Fermi level (Fig. 4 and Fig. 5).

For ZnSe, the valence band region of -3–0 eV is composed of Se 4p states, while the conduction band of 2–4 eV is mainly composed of the hybridization of Zn 4s and Se 4p states. The existence of electrons in the Zn 4s state in the conduction band indicates that the charge is transferred from Zn to Se; the presence of electrons in the Se 4p state in the conduction band signifies that the charge transfer is incomplete. Similar to the structure of ZnSe, the valence band near the Fermi level of $ZnS_{0.35}Se_{0.65}$ mainly comes from the p state of S/Se.

Due to the similarity of S and Se, the first-principles calculation results of ZnS_xSe_{1-x} pigment based on DFT establish that ZnS_xSe_{1-x} becomes a material with an adjustable optical bandgap. The color of the ZnS_xSe_{1-x} pigment can be varied by changing the component value *x*, and tunable color and optical properties can be

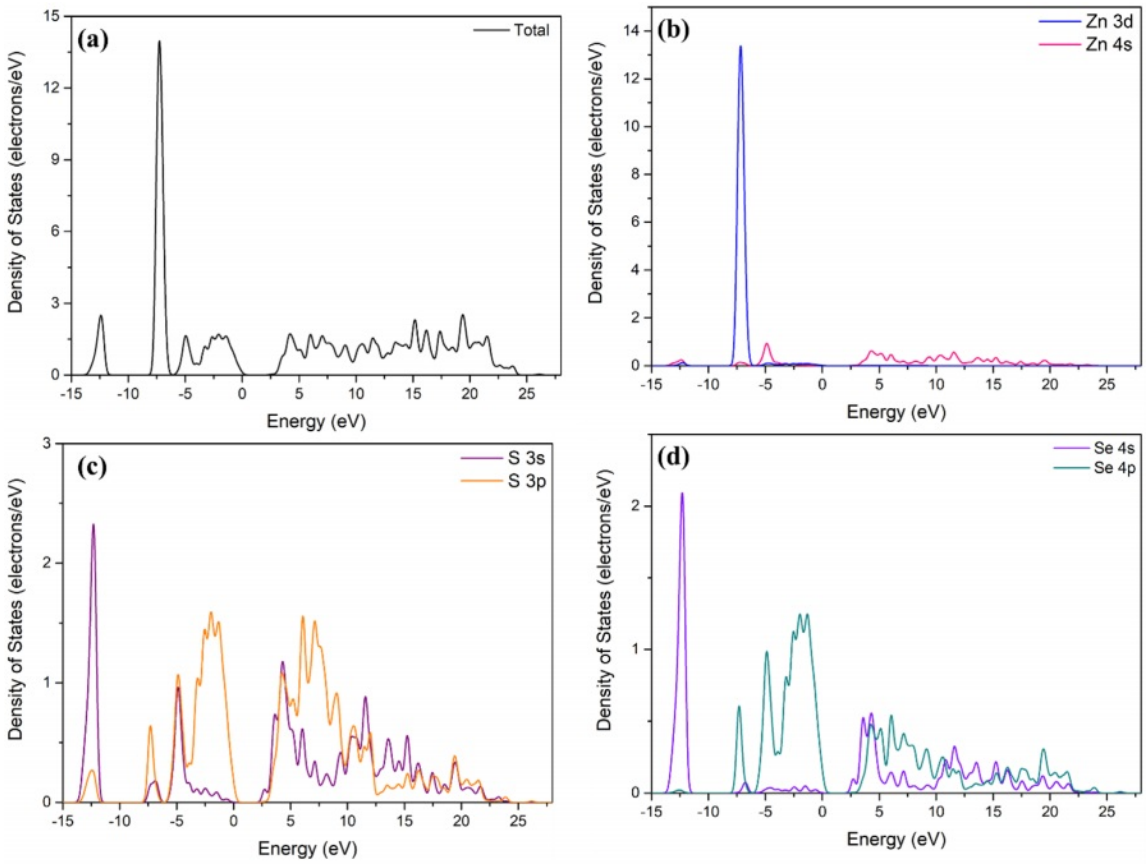

Fig. 5. Atom state density distribution of $ZnS_{0.35}Se_{0.65}$.

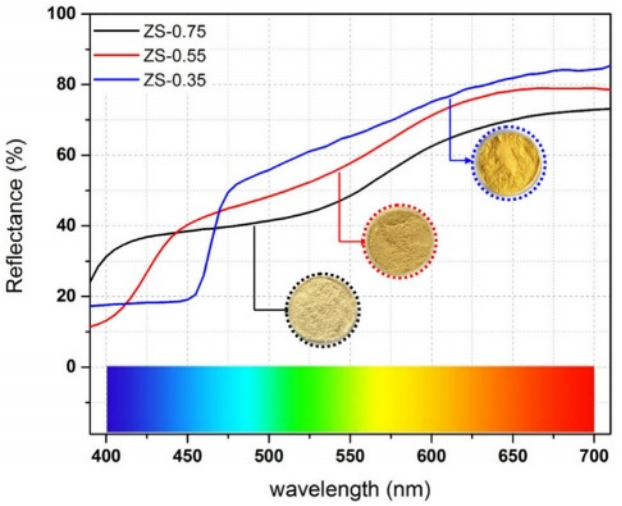

Fig. 6. Ultraviolet–visible diffuse reflectance spectra of ZnS_xSe_{1-x} pigments.

obtained (Fig. 6).

Kubelka–Munk optical properties

Fig. 6 displays the UV–vis diffuse reflectance spectra of ZnS_xSe_{1-x} pigments. The pigment reflectance in the UV–vis region rose varying degrees with increasing Se content in the ZnS_xSe_{1-x} pigments, so their color gradually changed from ivory white to bright yellow.

The Kubelka–Munk (K–M) model is used to describe the optical behavior of pigments in the visible light region. According to the K–M theory [27], the K–M transformed reflectance spectra are drawn from the UV–vis diffuse reflection spectra of ZnS_xSe_{1-x} pigments (Fig. 7).

The optical absorption edge of ZnS_xSe_{1-x} pigments shifts significantly from 394 ± 0.02 nm to a longer wavelength (i.e., 472 ± 0.03 nm) with rising Se content, representing that the sample can effectively reflect the yellow hue [Fig. 7 (a)]. With the changing of the anion composition x = [S]/([S] + [Se]), the continuous movement of the optical absorption edge further confirms the formation of ZnS_xSe_{1-x} solid solution in the pigment samples.

The calculated bandgap value and absorption wavelength of ZnS_xSe_{1-x} pigments are listed in Table 3. The E_g values of ZS-0.75, ZS-0.55, and ZS-0.35 samples are 3.21, 2.94, and 2.68 eV, respectively (the estimated error is ±0.02 eV). The shift of the optical absorption edge in the ZnS_xSe_{1-x} pigments and the resulting bandgap variation make the sample color gradually change from white to yellow (Fig. 6).

These results confirm that the ZnS_xSe_{1-x} pigments are materials with an adjustable optical bandgap. The color of ZnS_xSe_{1-x} pigments can be varied by changing the component value x, thereby obtaining tunable colors

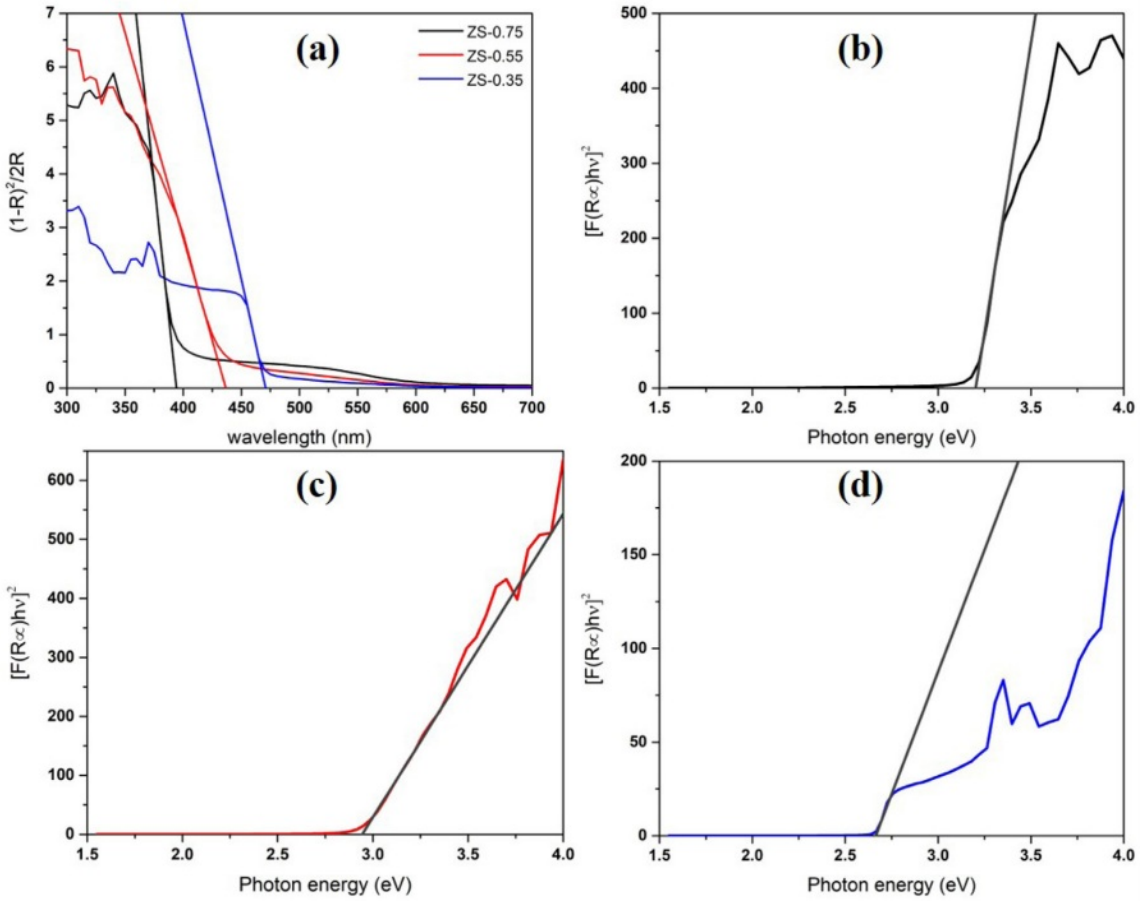

Fig. 7. Absorption edge calculated based on the Kubelka–Munk (K–M) theory (a), K–M transformed reflectance spectra (b), (c), and (d) of ZnS_xSe_{1-x} pigments.

and optical properties to meet visual and aesthetic requirements.

Analysis of Vegard's law for ZnS_xSe_{1-x}

Vegard's law [28] is used to explain the nonlinear changes in the optical bandgap and other physical properties of semiconductor alloy nanomaterials with changes in their composition. Vegard's law shows that the lattice parameters of a ternary solid solution tend to vary linearly with the changing composition, but other physical properties, such as optical bandgap [29], usually exhibit nonlinear changes. The bandgap value of ZnS_xSe_{1-x} pigments varies with the anion composition x = [S]/([S] + [Se]), which can be fitted to the quadratic function of x,

$$E_g(x) = xE_g(\mathrm{ZnS}) + (1-x)E_g(\mathrm{ZnSe}) - x(1-x)b \quad (4)$$

where E_g(ZnS), E_g(ZnSe), and $E_g(x)$ are the bandgap values of ZnS, ZnSe, and ZnS_xSe_{1-x} pigments, respectively, and b is the optical bowing constant. The bending constant b describes the degree of nonlinear changes in the optical bandgap.

In the ZnS_xSe_{1-x} ternary solid solution, changing the ratio between S^{2-} and Se^{2-} atoms leads to the redistribution of electrons in the atom, and the variation in the negative ion bond length adapts to the ZnS_xSe_{1-x} composition of each x value [30]. Studies by Swafford et al. [30] and Ingole et al. [31] have shown that the constant b is insensitive to lattice parameters. Therefore, the optical bandgap value of the ZnS_xSe_{1-x} pigments measured in Table 3 was fitted by Origin according to Vegard's law to obtain the value of b (Fig. 8). The dots in Fig. 8 are the experimental data, and the curve is the quadratic fitting based on the experimental results. The Origin's best fit is b = 0.815, consistent with the results reported

Table 3. Bandgap value and absorption wavelength of ZnS_xSe_{1-x} pigments.

Samples	ZS-0.75	ZS-0.55	ZS-0.35
Band gap E_g (ev) (estimated uncertainty: ± 0.02 eV)	3.21	2.94	2.68
Dominant wavelength λ (nm)	394 ± 0.02	437 ± 0.03	472 ± 0.03

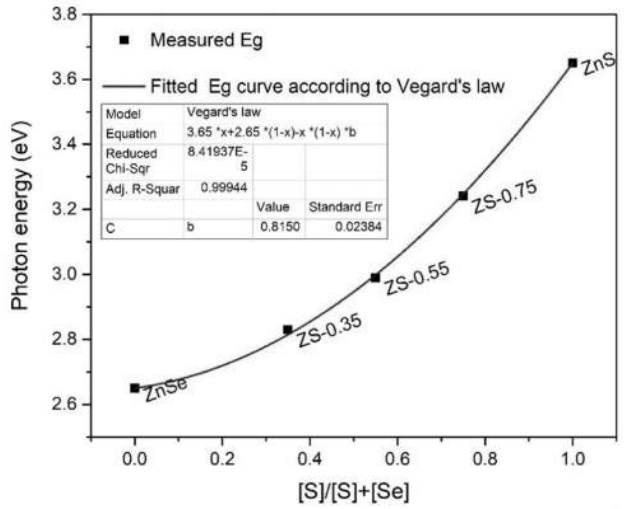

Fig. 8. Bandgap value of ZnS_xSe_{1-x} as a function of composition x (dots are the experimental data, and the curve is the quadratic fitting based on the experimental results).

by Dimitrievska et al. [21] and Chuo et al. [32].

In this study, a relatively small b value indicates that ZnSe and ZnS have excellent compatibility. Therefore, in the synthesis of ZnS_xSe_{1-x} pigments with different x component values, the predetermined optical bandgap can be adjusted by changing the molar ratio of S to Se in the raw materials so that the ZnS_xSe_{1-x} pigments can exhibit color changes (Fig. 6).

Conclusions

(1) The first-principles calculation results of ZnS_xSe_{1-x} pigment based on DFT show that ZnS_xSe_{1-x} transforms into a material with an adjustable optical bandgap due to the similarity of S and Se. The color of the ZnS_xSe_{1-x} pigment can be varied by changing the x component value, and tunable color and optical properties can be obtained.

(2) The Kubelka–Munk (K–M) model was used to describe the optical behavior of ZnS_xSe_{1-x} pigment in the visible light region. With increasing anion composition x = [S]/([S] + [Se]), the pigment lattice parameters increase, and the ZnS_xSe_{1-x} pigments' colors gradually changed from ivory white to bright yellow. The continuous movement of the optical absorption edge further confirms the formation of ZnS_xSe_{1-x} solid solution in the pigment samples.

(3) The Analysis of Vegard's law for ZnS_xSe_{1-x} shows that changing the ratio between S^{2-} and Se^{2-} atoms leads to the redistribution of electrons in the atom, and the variation in the negative ion bond length adapts to the ZnS_xSe_{1-x} composition of each x value. A relatively small optical bowing constant (b) value indicates that ZnSe and ZnS have excellent compatibility.

(4) The color of ZnS_xSe_{1-x} pigments can be varied by changing the x component value, thereby obtaining tunable colors and optical properties to meet visual and aesthetic requirements.

Acknowledgements

This work was supported by the Guangdong Basic and Applied Basic Research Foundation (No. 2021A1515110487) and Natural Science Foundation of Guangxi (2024GXNSFAA010520).

References

1. S. Jamshidi, S. Rasouli, B. Janipour, and B. Mirhadi, J. Ceram. Process. Res. 16 (2015) 667-673.
2. W. Chatjuthamanee, R. Muanghlua, B. Boonchom, and N. Vittayakorn, J. Ceram. Process. Res. 13 (2012) 713-716.
3. B. Tanisan and S. Turan, J. Ceram. Process. Res. 12 (2011) 462-467.
4. Y.Z. Halefoglu and E. Kusvuran, J. Ceram. Process. Res. 11 (2010) 92-95.
5. J. Zhang, Y.M. Park, X.Y. Tan, M.K. Bae, D.J. Kim, T.H. Jang, M.S. Kim, S.W. Lee, and T.G. Kim, J. Ceram. Process. Res. 20 (2019) 589-596.
6. J.H. Lee, H.J. Hwang, J.W. Kwon, J.H. Kim, K.T. Hwang, and K.S. Han, J. Ceram. Process. Res. 20 (2019) 127-132.
7. L.L. Wang, X.X. Liu, X.P. Li, X.F. Wang, L.N. Feng, and X.R. Hou, J. Ceram. Process. Res. 22 (2021) 240-245.
8. K.R. Pyon, K.S. Han, and B.H. Lee, J. Ceram. Process. Res. 12 (2011) 279-288.
9. S. Rasouli, M. Valefi, S.J. Moeen, and A.M. Arabi, J. Ceram. Process. Res. 12 (2011) 450-455.
10. S. Rasouli, J. Ceram. Process. Res. 12 (2011) 668-672.
11. M. Suwan, P. Premjit, P. Thavorniti, P. Kidkhunthod, S. Supothina, J. Ceram. Process. Res. 18 (2017) 10-15.
12. T.N. Rao, I. Hussain, Riyazuddin, and B.H. Koo, J. Ceram. Process. Res. 20 (2019) 411-417.
13. M. Ullah, H.J. Kim, J.G. Heo, D.K. Roh, and D.S. Kim, J. Ceram. Process. Res. 20 (2019) 86-91.
14. R. Azizi, S. Rasouli, N.P. Ahmadi, A.J.J. Kolaei, and M. Azizie, J. Ceram. Process. Res. 13 (2012) 164-169.
15. N. Gurbuz, E. Coskun, and E. Ozel, J. Ceram. Process. Res. 11 (2010) 184-190.
16. W. Zhou, J. Ye, Z. Liu, L. Wang, L. Chen, S. Zhuo, Y. Liu, and W. Chen, Inorg. Chem. (2021).
17. X. Tian, Z. Chen, J. Wen, Y. Du, J. Hu, S. Wang, H. Peng, J. Li, and Y. Peng, J. Ceram. Process. Res. 18 (2017) 116-121.
18. M.R. Bodke, Y. Purushotham, and B.N. Dole, J. Ceram. Process. Res. 16 (2015) 601-604.
19. K. Liu, W. Song, Y. Xu, J. Li, and Z. Wang, J. Ceram. Process. Res. 19 (2018) 146-149.
20. S.D. Yoon, J.W. Yun, and Y.H. Yun, J. Ceram. Process. Res. 21 (2020) 479-487.
21. M. Dimitrievska, H. Xie, A.J. Jackson, X. Fontane, M. Espindola-Rodriguez, E. Saucedo, A. Perez-Rodriguez, A. Walsh, and V. Izquierdo-Roca, PCCP 18 (2016) 7632-7640.
22. X.L. Guo, Q.L. Rao, L.L. Li, Y. Zou, and C. Wu, J. Ceram. Process. Res. 17 (2016) 815-817.
23. K. Petzke, Physica B 273-274 (1999) 866-869.
24. W.K. Jung, J.W. Hong, and D.H. Choi, J. Ceram. Process. Res. 22 (2021) 86-90.
25. J. Zhou and X. Wu, J. Alloys Compd. 695 (2017) 1392-

1396.
26. J.P. Perdew, Int. J. Quantum Chem. 28 (1985) 497-523.
27. P. Kubelka and F. Munk, Zeitschrift fur Technische Physik 12 (1931) 593-601.
28. L. Vegard, Zeitschrift für Physik 5 (1921) 17-26.
29. P. Jitti-a-porn, S. Suwanboon, P. Amornpitoksuk, and O. Patarapaiboolchai, J. Ceram. Process. Res. 12 (2011) 85-89.
30. L.A. Swafford, L.A. Weigand, M.J. Bowers, J.R. McBride, J.L. Rapaport, T.L. Watt, S.K. Dixit, L.C. Feldman, and S.J. Rosenthal, J. Am. Chem. Soc. 128 (2006) 12299-12306.
31. P.P. Ingole, G.B. Markad, D. Saraf, L. Tatikondewar, O. Nene, A. Kshirsagar, and S.K. Haram, The Journal of Physical Chemistry C 117 (2013) 7376-7383.
32. H.X. Chuo, T.Y. Wang, and W.G. Zhang, J. Alloys Compd. 606 (2014) 231-235.

Appendix A.

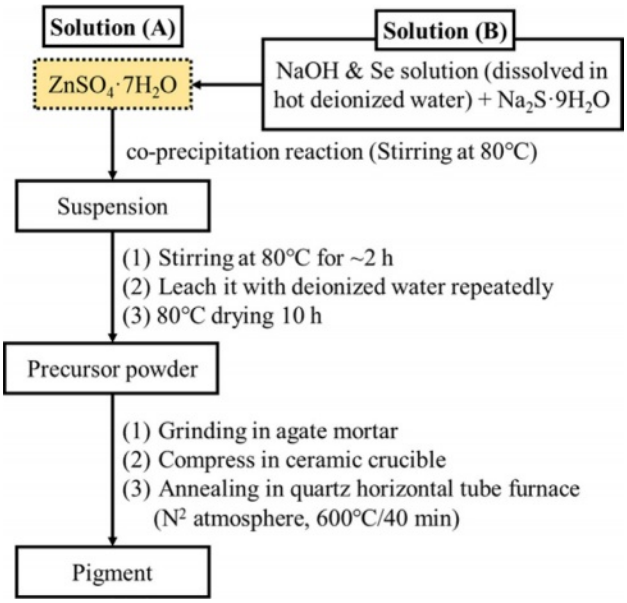

Fig. A1. Flowchart for synthesis procedure of ZnS_xSe_{1-x} pigments.

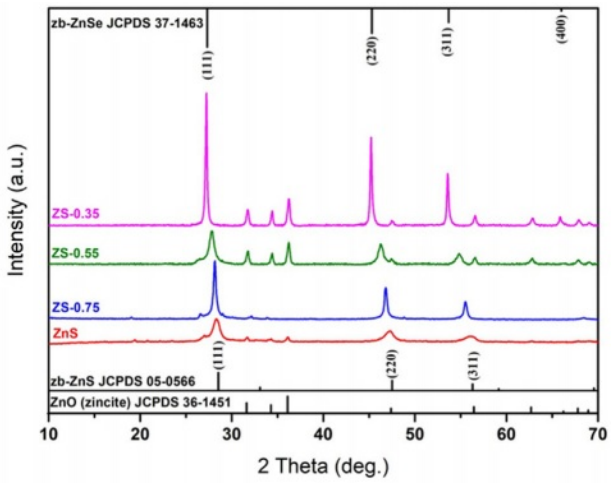

Fig. A2. X-ray diffraction patterns of ZnS_xSe_{1-x} (x = 1, 0.75, 0.55, and 0.35) pigments.

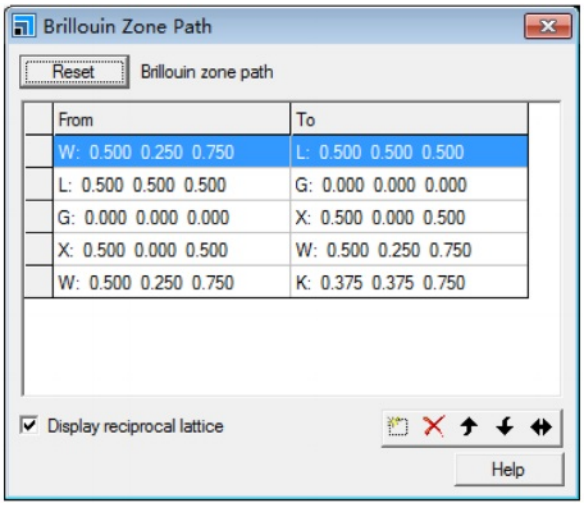

Fig. A3. Selection rules for high-symmetry points of the Brillouin zones of $ZnS_{0.35}Se_{0.65}$ structure.

Table A1. Compositions of ZnS_xSe_{1-x} precursors.

Sample		Precursor atomic ratio Zn:S:Se
ZnS_xSe_{1-x}	ZnS	1:1:0
	ZS-0.75	1:0.75:0.25
	ZS-0.55	1:0.55:0.45
	ZS-0.35	1:0.35:0.65